Breast Tumor Detection Ability of a Planar Microwave Imaging System

Tommy Henriksson *Student Member, IEEE,* Nadine Joachimowicz, Bernard Duchêne and Jean-Charles Bolomey *Fellow Member, IEEE*

***Abstract*—This paper deals with the breast tumor detection ability of a planar microwave imaging system. Indeed, microwave imaging seems to have a significant potential in such a biomedical application. By means of a numerical model based upon electric field volume integral equations, we investigate the influence of several parameters, such as the respective sizes of the breast and the tumor, the operating frequency and the electromagnetic properties of the different media, on the detection ability. The latter is estimated by comparing the scattered fields observed in the presence and in the absence of tumor and by accounting for the signal to noise ratio available with the experimental setup developed at the laboratory.**

***Index Terms*—Breast Cancer Detection, Microwave Imaging.**

I. Introduction

DURING the last decade, many research efforts have been devoted to achieve a microwave modality for the early detection of breast cancer [1]–[7]. Indeed, early studies [8] have evidenced that, in the microwave frequency range, tumors show a strong dielectric contrast with respect to healthy tissues, which brings hope for better detection capabilities with microwaves than with usual imaging means such as X rays or ultrasounds. Hence, various experimental systems [1]–[4] and imaging algorithms [4]–[7], [9] have been considered. Several groups have already obtained promising results, using both radar-based [2] and inverse scattering algorithms [10].

We are concerned, herein, with the feasability of a new planar three-dimensional microwave mammography set-up which could be an extension of an existing planar 2.45 GHz microwave camera [4]. The purpose of this paper is to estimate the ability of this system to detect tumors in breast tissues. We investigate the influence of some geometric and electromagnetic parameters, such as the operating frequency, the breast immersion medium (denoted as host or coupling medium), the breast tissue and the size of the tumor with respect to that of the breast phantom. The tumor detection ability of the system, henceforth denoted as TDA, is estimated by means of a numerical model based upon electric field volume integral equations whose discrete versions are obtained by applying a method of moments. The TDA of the system is then deduced from the mean square norm of the difference between the fields measured on a sensor line in the presence and in the absence of the tumor, respectively. A detection threshold is then defined by accounting for the experimental signal to noise ratio available with the existing microwave camera.

The authors are with the Département de Recherche en Électromagnétisme, Laboratoire des Signaux et Systèmes (UMR 8506, CNRS - Supelec - Univ. Paris-Sud 11), Gif-sur-Yvette, France (e-mail: Tommy.Gunnarsson@lss.supelec.fr). T. Henriksson is also with the School of Innovation, Design and engineering, Malardalen University.

II. The Experimental Set Up

Figure 1 displays the planar microwave camera which has been already extensively described in [4], [11] and [12]. The object under test is immersed in a 20 cm wide water tank located in between two 30×30 cm apertures horn-antennas operating at a 2.45 GHz frequency. The incident field radiated by the emitting horn antenna can be considered as a plane wave of limited extent due to an appropriate horn profiling and to the presence of dielectric lenses. As well known, the advantage of using water as coupling medium rather than air is threefold: i) the spatial resolution is approximately improved by a factor 10 with the former as compared with the latter due to wavelength reduction in water, ii) the wave impedance of water is closer to that of biological tissues than the impedance of air, which reduces reflection losses and improves the penetration of waves within biological objects and iii) the high losses in water reduce the object-system interactions that are usually not taken into account in the reconstruction algorithms and, hence, the artifacts resulting from model errors that could appear in the retrieved images.

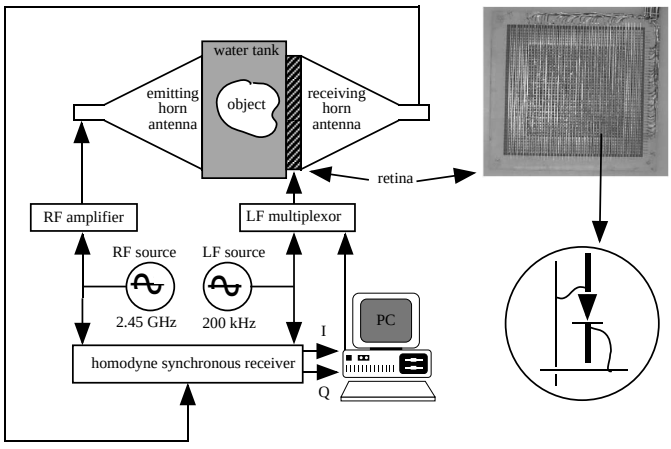

Fig. 1. The principles ot the 2.45 GHz microwave camera (left), a front view of the 2D retina (top - right) and the details of one of its 32×32 elements: a dipole loaded by a PIN diode (down - right).

The scattered fields are measured by means of the Modulated Scattering Technique [11] thanks to a retina placed in front of the receiving horn antenna (collector) and whose details are displayed in Figure 1. The retina consists of an

array of 32×32 dipoles loaded by PIN diodes modulated at a low frequency (200 kHz). The collector measures the modulated fields re-radiated by the dipoles. This technique avoids any complex microwave multiplexor and allows a fast electronic scanning of the fields. From these fields, images of the equivalent current distribution (that depends upon the electromagnetic properties of the object) in any cross section of the object can be retrieved rapidly. Indeed, the most recent developments of the planar microwave camera were focused on the realization of a quasi-real time imaging system that can be used to study dynamic phenomena. Benefiting from the spectacular increase of microcomputer performances and of some acquisition and control system transformations, the camera is now able to produce quasi-real time (i.e., at a rate of 25 images/s) qualitative images by using a spectral reconstruction technique [4]. While loosing the real time capacity of the system, the quality of the images can be enhanced by using multi-view data obtained by varying the direction of illumination or, equivalently, by rotating the object.

III. A Two-Dimensional Numerical Tool

A. The configuration

Figure 2 shows the 2D configuration used for TDA assessement and compatible with the cylindrical nature of the phantom used in a previous experiment [13]. The latter consists of a breast affected with an off-centered tumor-like anomaly (Figure 2). The breast, immersed in a host medium, is illuminated by a TM polarized plane wave whose electric field is parallel to the phantom axis and whose implicit time dependence is chosen as $exp(-i\omega t)$, ω being the angular frequency. The different media are characterized by their propagation constant k_a and complex relative permittivity $\varepsilon_a^* = \varepsilon_a' + i\varepsilon_a''$, where subscript a stands for 1 in the host medium, b in the breast and t in the tumor. The breast and the tumor have circular cross-sections with diameters D and d that vary in the ranges $6 < D < 12$ cm and $0.1 < d < 3$ cm, respectively, whereas the tumor off-set is fixed to 2.3 cm. Let us note that L = 36 views are realized at varying incidence angle θ, each view consisting of M = 32 measurements of the scattered fields on a sensor line perpendicular to the propagation direction of the incident wave and located at a distance of 10 cm from the breast centre, with a 7.21 mm sampling step, i.e., half the wavelength in water.

The goal is to study the influence of several parameters (i.e., the operating frequency, the nature of the external host medium and the size and the electromagnetic parameters of the breast tissue-like medium) on the TDA of the microwave imaging system. The latter is estimated by comparing the scattered fields computed on the sensor line in the presence and in the absence of the tumor-like anomaly.

B. Two-Dimensional Modeling

The simulated data are obtained by means of a 2D scalar electromagnetic direct solver which computes the scattered field $E^{scat}(r)$ on a sensor line, when the incident field $E^{inc}(r)$ and the phantom Ω are known. The phantom is described by its relative permittivity distribution $\varepsilon^*(r)$, such that $\varepsilon^*(r) = \varepsilon_b^*$ when r is located in the breast or $\varepsilon^*(r) = \varepsilon_t^*$ when it is located in the tumor, and we define k_Ω and k_1, the propagation constants in the object and in the host medium, respectively, such that:

$$k_\Omega^2(\boldsymbol{r}) = \omega^2 \mu_0 \varepsilon_0 \varepsilon^*(\boldsymbol{r}) \tag{1}$$

$$k_1^2 = \omega^2 \mu_0 \varepsilon_0 \varepsilon_1^* \tag{2}$$

whith ε_0 and μ_0 the dielectric permittivity and the magnetic permeability of vacuum, respectively, and the object function $\chi(\boldsymbol{r})$ as:

$$\chi(\boldsymbol{r}) = k_\Omega^2(\boldsymbol{r}) - k_1^2. \tag{3}$$

The scattered field E^{scat} is defined as the difference between the total field E^{tot} measured in the presence of the object and the incident field E^{inc} measured in the absence of the latter. By applying Green's theorem to the Helmholtz wave equations satisfied by these fields and by accounting for the continuity and radiation conditions, we get two coupled electric field integral equations. The first one, the so-called observation equation, expresses the scattered field as radiated by the equivalent currents (or Huygens type sources) $J(\boldsymbol{r})$ induced in the object by the incident wave ($J(\boldsymbol{r}) = \chi(\boldsymbol{r}) E^{tot}(\boldsymbol{r})$); it reads:

$$E^{scat}(\boldsymbol{r}) \;=\; \int_\Omega G(\boldsymbol{r}, \boldsymbol{r}')\; \chi(\boldsymbol{r}')\; E^{tot}(\boldsymbol{r}')\; \mathrm{d}\boldsymbol{r}' \tag{4}$$

where $G(\boldsymbol{r}, \boldsymbol{r}')$ is the 2D Green's function which represents the field radiated by a line source located at the source point $\boldsymbol{r}'$ and observed at point $\boldsymbol{r}$ in the absence of the object. The latter reads $G(\boldsymbol{r}, \boldsymbol{r}') = \mathrm{i} H_0^1(k_1 |\boldsymbol{r} - \boldsymbol{r}'|)/4$, with H_0^1 the zero order Hankel function of the first kind.

The second equation, the so-called coupling or state equation, expresses the total field within the object in the same way:

$$E^{tot}(\boldsymbol{r}) \;=\; E^{inc}(\boldsymbol{r}) + \int_\Omega G(\boldsymbol{r}, \boldsymbol{r}')\; \chi(\boldsymbol{r}')\; E^{tot}(\boldsymbol{r}')\; \mathrm{d}\boldsymbol{r}'. \tag{5}$$

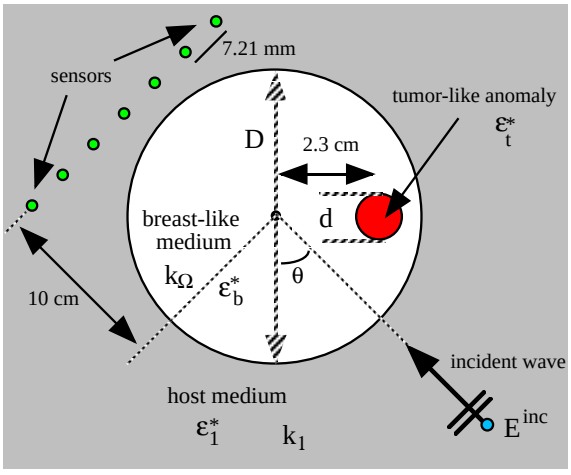

Fig. 2. The geometry of the 2D configuration.

The direct solver deals with discrete counterparts of the above equations obtained by applying a moment method with pulse basis functions and point matching [14]. This results in partitioning the object domain in N elementary square pixels small enough in order to consider the permittivity and the total field as constant over each of them, a pixel side of $\lambda/10$ (with λ = wavelength in the host medium) being usually sufficient to ensure convergence in field computations. The discrete equations then read:

$$E^{tot}(\boldsymbol{r}_j) = E^{inc}(\boldsymbol{r}_j) + \sum_{n=1}^{N} \mathcal{G}_{jn}\ \chi(\boldsymbol{r}_n)\ E^{tot}(\boldsymbol{r}_n) \quad \text{for } j = 1, 2, ..., N \tag{6}$$

$$E^{scat}(\boldsymbol{r}_m) = \sum_{n=1}^{N} \mathcal{G}_{mn}\ \chi(\boldsymbol{r}_n)\ E^{tot}(\boldsymbol{r}_n) \quad \text{for } m = 1, 2, ..., M. \tag{7}$$

$\mathcal{G}_{jn}$ and $\mathcal{G}_{mn}$ result from the integration of the Green's function over the elementary square pixels and can be approximated by analytic expressions obtained by replacing the square pixels by discs of same area [15]. The direct solver first solves (6) for E^{tot}. This is done directly by means of a Gauss-Jordan inversion algorithm as it does not pose any ill-conditioning problem and as the size of the object is not too large as compared to the wavelength. For larger object, a Conjugate Gradient Fast Fourier Transform method (CG-FFT, [16]) could be used with profit as it preserves the convolutional nature of the equations and, hence, allows to save time. Then (7) is solved for E^{scat}, which can be done straightforwardly. Let us note that these two steps have to be repeated for each view at varying incidence.

C. Breast Phantom Electromagnetic Properties

Many studies have been already focused on the electromagnetic characterization of normal and cancerous breast tissues [17]–[20]. However, since the tissue composition is complex, a large-scale study, covering a wide frequency band, has not been done before Lazebnik *et al.* [21], who have recently reported that the normal breast tissues may be partitioned into three different groups, depending upon their fat content. At 2.45 GHz, these three groups are as follows: i) from 0 to 30% of adipose tissue, the real and imaginary parts of the dielectric permittivity read $\varepsilon'_b = 47$ and $\varepsilon''_b = 12$, respectively, ii) from 31% to 84% of adipose tissue, they read $\varepsilon'_b = 38$ and $\varepsilon''_b = 9$, respectively, and iii) from 85% to 100% of adipose tissue, they read $\varepsilon'_b = 5$ and $\varepsilon''_b = 0.5$. It can be noted that, in order to take into account the fact that the breast can be a mixture of the three types of tissues distinguished above, we introduce, in the numerical study, a fourth type with a permittivity value ($\varepsilon'_b = 35$, $\varepsilon''_b = 5$) that corresponds to an average of the three above complex permittivities. As for the cancerous tissues, a good estimation of their complex permittivity at the same frequency is approximately ($\varepsilon'_t = 65$, $\varepsilon''_t = 14$), which is the value used herein. This leads to a real contrast C between normal and cancerous breast tissues ($C = \varepsilon'_t/\varepsilon'_b$) ranging from $C = 13$ for a highly adipose tissue to around $C = 1.5$ for a lowly adipose one [22].

IV. Numerical results

A. A TDA criterion

The goal is now to analyze the appropriateness of the planar camera for tumor detection and to determine the main parameters that impact on the TDA of the system. The various geometric and electromagnetic parameters are set according to Figure 2. Let us note that, once computed, the scattered fields are systematically corrupted by an additive 40 dB SNR gaussian noise which is in the range of the noise that is experimentally observed with the camera. Indeed, the signal to noise ratio has been estimated at 30 dB when the field is evaluated from a single shot measurement and at 55 dB when the latter is obtained through an average of 500 samples. Hence, in the following, the simulated noise is expected to account for both model errors and measurement noise. Then a TDA criterion can be defined as the mean-square difference of the scattered fields computed in the absence (E_b^{scat}) and in the presence (E_t^{scat}) of the tumor:

$$TDA = \frac{\sum_{l=1}^{L}\sum_{m=1}^{M} |E_t^{scat}(\boldsymbol{r}_m) - E_b^{scat}(\boldsymbol{r}_m)|^2}{\sum_{l=1}^{L}\sum_{m=1}^{M} |E_b^{scat}(\boldsymbol{r}_m)|^2}. \tag{8}$$

In order to quantify the noise impact on the detection ability, the TDA has been calculated by replacing the scattered field in the presence of tumor E_t^{scat} by the scattered field in the absence of tumor E_b^{scat} corrupted by an additive noise. It was found that the TDA corresponding to a 40 dB SNR gaussian noise is 1%. Moreover, the definition of a significant threshold for the TDA must also account for the image reconstruction process. For example, it was observed that a TDA larger than about 10% was required to obtain an acceptable quality for the images obtained by means of a Newton-Kantorovich inversion algorithm [9]. Consequently, in the following, the detection threshold has been fixed to a TDA of 10%.

B. Influence of the Contrast and Losses of Breast-Like Tissues

Figure 3 displays the results obtained for different values of the breast tissue-like medium contrast and losses, for $D = 10$ cm and $d = 1.5$ cm. As it can be observed, the TDA is sensitive to both the contrast and the losses and decreases as both of them increase. Furthermore, whatever the contrast, when the imaginary part of the complex permittivity becomes larger than 15, the tumor is no more detectable. Note that the numerical study reported in this section has been performed simultaneously with an experimental investigation of the TDA measured by means of the microwave camera on a phantom with the same geometrical parameters as above, the tumor being then replaced by a metallic rod and the breast-like medium by water of varying salinity [13] and the same conclusions can be inferred in both cases; as the latter varies from 2.5 g/l to 10 g/l, which corresponds to a range of variation of losses such that $10.5 < \varepsilon''_b < 21.9$ according to the

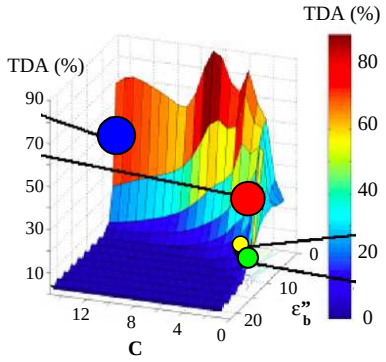

Fig. 3. Effect of contrast C ($C = \varepsilon_1'/\varepsilon_b'$) and losses ($\varepsilon_b''$) of the breast tissue-like phantom immersed in water at 37°C on the TDA in conditions similar to the experimental configuration of the camera. The colored circles indicate the four types of breast tissues: i) green = $0-30\%$ adipose tissues, ii) yellow = $31-84\%$ adipose tissues, iii) blue = $85-100\%$ adipose tissues and iv) red = averaged tissue with ($\varepsilon_b' = 35,\ \varepsilon_b'' = 5$).

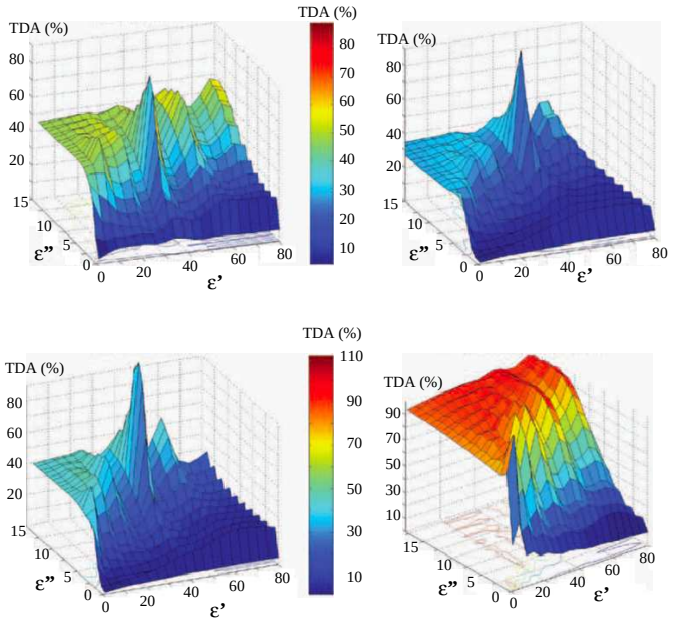

Fig. 4. Effect of the coupling medium properties on the TDA in conditions similar to the experimental configuration of the camera, for different breast-like tissues: i) top-left = mean breast-like medium (ε_b' = 35.0, ε_b'' = 5.0), ii) top-right = $0-30\%$ adipose medium (ε_b' = 47.0, ε_b'' = 12.0), iii) bottom-left = $31-84\%$ adipose medium (ε_b' = 38.0, ε_b'' = 9.0) and iv) bottom-right = $85-100\%$ adipose medium (ε_b' = 5.0, ε_b'' = 0.5).

Stogryn's model [23] at a temperature of 37°C, the metallic rod, whose presence can be observed for low losses, becomes invisible.

Furthermore, the four breast tissue types with different adipose contents considered in section III-C correspond to TDA greater than the detection threshold of 10%.

The results displayed in Figure 4 concern the influence of the host medium permittivity on the detection of the tumor for different breast-like tissues. As it can be observed, the response levels differ a lot according to the characteristics of the breast phantom: the higher the fat content, the higher is the TDA. Moreover, it appears that whatever the breast tissue considered, the TDA increases with the host medium losses. Note that the sharp spikes that appear except for higly adipose tissues correspond to the case where the host medium as the same complex permittivity as the breast tissue. Finally, according to Figure 4, we can estimate an appropriate range for the dielectric properties of the host medium: namely, ε' must lie around 30 and ε'' must be greater than 7. Note that, although the real part of its permittivity is twice higher than the above value, tap water used in the microwave planar set-up remains a possible candidate as coupling medium, especially from highly adipose breast tissues. Indeed, its values of permittivity, computed according to the Stogryn's model at a temperature of $37°C$ by assuming a salinity of 0.4 g/l of NaCl salt, are about ε' = 73.4 and ε'' = 7.2,

C. Influence of the Operating Frequency

Hence, in this section, tap water in the same conditions (ε' = 73.4, ε'' = 7.2) is considered as coupling medium. Figure 5 displays the TDA as a function of the breast tissue characteristics at 500 MHz and 900 MHz and can be directly compared to Figure 3 corresponding to 2.45 GHz. As it can be observed from Figures 5 and 3, the TDA increases with the frequency and, whatever the frequency, it decreases when the losses increase in the breast.

However, as evidenced in Figure 6, the permittivity of the breast tissues change with frequency; for tissues with low

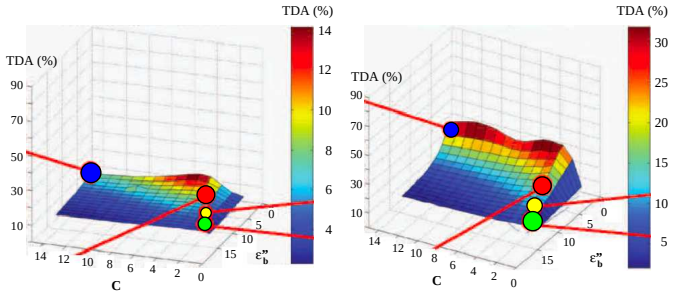

Fig. 5. Effect of contrast C ($C = \varepsilon_1'/\varepsilon_b'$) and losses ($\varepsilon_b''$) of the breast tissue-like phantom immersed in water at 37°C on the TDA at 500 MHz (left) and 900 MHz (right) for a 16 mm tumor-like anomaly. The colored circles indicate the four types of breast tissues: i) green = $0-30\%$ adipose tissues, ii) yellow = $31-84\%$ adipose tissues, iii) blue = $85-100\%$ adipose tissues and iv) red = averaged tissue with ($\varepsilon_b' = 35,\ \varepsilon_b'' = 5$).

and medium adipose contents, above 3 GHz losses increase with the frequency, whereas below 2 GHz they increase when the frequency decreases. As a consequence, the response of these tissues is lower than the detection threshold, even at a 900 MHz frequency. Hence, whatever be the fat content of the breast tissue, the operating frequency of the camera (i.e., 2.45 GHz) appears to be a good choice in terms of TDA.

D. Influence of the Tumor and Breast Sizes

Figure 7 displays the TDA as a function of the breast and tumor sizes for the four breast tissue types. In this case we consider a cylindrical breast phantom whose diameter ranges in between 6 cm and 12 cm and a tumor-like anomaly whose size ranges from 0.1 cm to 3 cm. As expected, the response increases with the size of the tumor and, except for the highly

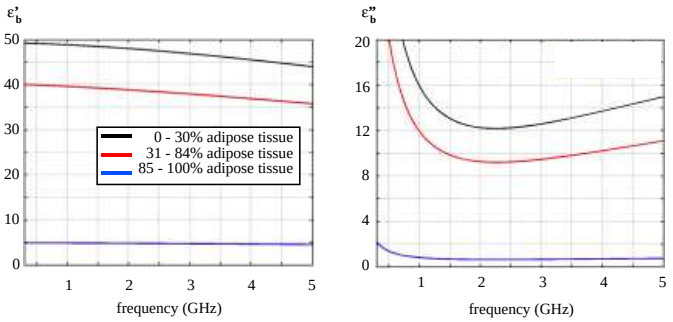

Fig. 6. The real (left) and imaginary (right) parts of the healthy breast tissue relative permittivity as a function of the frequency for different adipose contents according to [22].

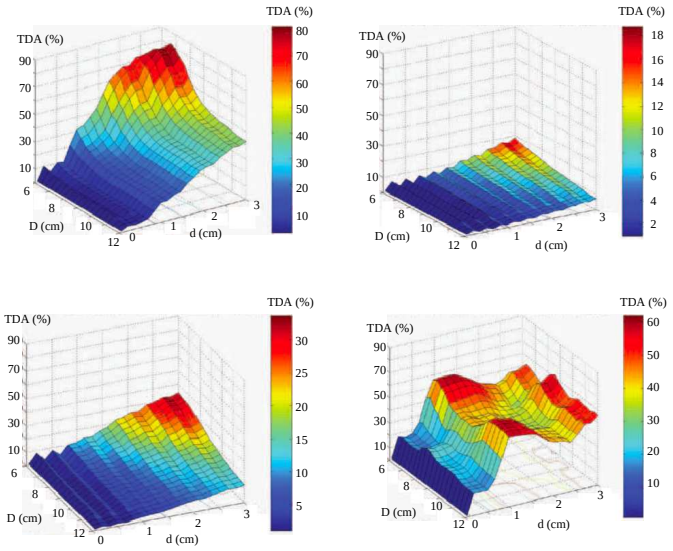

Fig. 7. Effect of the breast and tumor sizes (D and d, respectively) on the TDA at 2.45 GHz for a fixed host medium ($\varepsilon' = 73.37$, $\varepsilon'' = 7.16$) and for different breast-like tissues: i) top-left = mean breast-like medium ($\varepsilon'_b = 35.0$, $\varepsilon''_b = 5.0$), ii) top-right = $0-30\%$ adipose medium ($\varepsilon'_b = 47.0$, $\varepsilon''_b = 12.0$), iii) bottom-left = $31-84\%$ adipose medium ($\varepsilon'_b = 38.0$, $\varepsilon''_b = 9.0$) and iv) bottom-right = $85-100\%$ adipose medium ($\varepsilon'_b = 5.0$, $\varepsilon''_b = 0.5$).

adipose breast tissue, decreases as the breast size increases. Indeed, whatever the size of the breast in the limit of those considered in this study, a high TDA is obtained for highly adipose tissues. Thus, in the latter type of tissues, a 2 mm tumor appears to be possibly detectable in the experimental conditions of the microwave camera. As for the other tissue types, the minimal size for a tumor to be possibly detected depends upon the losses in the breast; hence, with $D = 10$ cm, the latter varies from 1 cm for an averaged tissue to 1.8 cm for a lowly adipose one.

V. Conclusion

This paper reports a preliminary sensitivity study on the breast tumor detection ability of a planar microwave imaging system developed at the laboratory. As a first remark, it can be noted that, although they have not be chosen in view of this particular application, two of the basic features of the microwave camera seem compatible with this use, i.e., the coupling medium and the operating frequency. The coupling medium consists in water which presents not only the previously reported threefold advantage of an immersion technique (better spatial resolution, improved penetration, reduced object-system interactions), but, in addition, exibits a relative complex permittivity close to the optimal operating conditions suggested by the TDA sensitivity assessement, although its real part is twice the desired value. The 2.45 GHz operating frequency is close to the frequency for which lowly and medium adipose breast tissues show minimal losses. Hence, this frequency is expected to provide a good penetration in most of the breast tissues and, hence, the possibility to detect deep-seated breast tumors. As for the other features whose influence has been studied herein, i.e., the electromagnetic and geometric parameters of breast and tumor, we have explored ranges of variation that cover the most of the situations that can be clinically encountered. From this study, it comes out that the TDA is very sensitive to the breast size and losses and, of course, to the size of the tumor. Hence the minimal size for a tumor to be possibly detected depends upon the size and the fat content of the breast; for instance, for a 10 cm sized breast of medium adipose tissue, a 1.5 cm tumor appears to be detectable with the existing planar microwave camera. Possible improvements of the camera system dedicated to breast tumor detection are currently investigated.

References

[1] P. M. Meaney, M. W. Fanning, D. Li, S. P. Poplack, and K. D. Paulsen, "A clinical prototype for active microwave imaging of the breast," *IEEE Trans. Microwave Theory Tech.*, vol. MTT-48, no. 11, pp. 1841–1853, 2000.

[2] X. Li, S. K. Davis, S. C. Hagness, D. W. van der Weide, and B. D. V. Veen, "Microwave imaging via spacetime beamforming: experimental investigation of tumor detection in multilayer breast phantoms," *IEEE Trans. Microwave Theory Tech.*, vol. MTT-52, no. 8, pp. 1856–1865, 2004.

[3] G. Bindu, S. J. Abraham, A. Lonappan, V. Thomas, C. K. Aanandan, and K. T. Mathew, "Active microwave imaging for breast cancer detection," in *PIER Progress In Electromagnetic Research*, J. A. Kong, Ed. Cambridge: EMW Publishing, 2006, vol. 58, pp. 149–169.

[4] A. Joisel and J.-C. Bolomey, "Rapid microwave imaging of living tissues," in *Proc. SPIE Int. Symp. Medical Imaging*, San Diego, 2000, pp. 320–330.

[5] M. Miyakawa, T. Ishida, and M. Watanabe, "Imaging capability of an early stage breast tumor by CP-MCT," in *Proc. 26th IEEE EMBS Int. Conf.*, San Francisco, 2004.

[6] D. Li, P. M. Meaney, and K. D. Paulsen, "Conformal microwave imaging for breast cancer detection," *IEEE Trans. Microwave Theory Tech.*, vol. MTT-51, no. 4, pp. 1179–1186, 2003.

[7] E. C. Fear, X. Li, and S. C. Hagness, "Conformal microwave imaging for breast cancer detection," *IEEE Trans. Biomed. Eng.*, vol. BE-49, no. 8, pp. 812–822, 2002.

[8] W. T. Joines, R. L. Jirtle, M. D. Rafal, and D. J. Schaefer, "Microwave power absorption differences between normal and malignant tissue," *Int. J. Radiation Oncology Biol. Phys.*, vol. 6, pp. 681–687, 1980.

[9] N. Joachimowicz, C. Pichot, and J. P. Hugonin, "Inverse scattering: an iterative numerical method for electromagnetic imaging," *IEEE Trans. Antennas Propag.*, vol. AP-39, no. 12, pp. 1742–1752, 1991.

[10] W.-K. Chen, K. D. Paulsen, P. M. Meaney, and L. Gilman, "Alternative breast imaging: four model-based approaches," in *Series in Eng. and Computer Science*. Springer, 2005, vol. 778.

[11] J.-C. Bolomey and F. Gardiol, *Engineering Applications of the Modulated Scatterer Technique*. Boston: Artech House, 2001.

[12] J.-C. Bolomey, "Modulated probe arrays for rapid antenna testing; principle and applications," *Electronics/communications HF*, vol. 2, pp. 35–46, 1997.

[13] T. Henriksson, N. Joachimowicz, C. Conessa, and J.-C. Bolomey, "Quantitative microwave imaging for breast cancer detection using a planar 2.45 GHz system," *submitted to IEEE Trans. Instrum. Meas.*, april 2009.
[14] W. C. Gibson, *The Method of Moments in Electromagnetics*. Boca Raton: Chapman & Hall/CRC, 2007.
[15] J. Richmond, "Scattering by a dielectric cylinder of arbitrary cross-section shape," *IEEE Trans. Antennas Propag.*, vol. AP-13, no. 3, pp. 334–341, 1965.
[16] T. K. Sarkar, E. Arvas, and S. M. Rao, "Conjugate gradient method for the solution of electromagnetic radiation from electrically large and small conducting bodies," *IEEE Trans. Antennas Propag.*, vol. AP-34, no. 5, pp. 635–640, 1986.
[17] S. S. Chaudhary, R. K. Mishra, A. Swarup, and J. M. Thomas, "Dielectric properties of normal and malignant human breast tissues at radiowave and microwave frequencies," *Indian J. Biochem. Biophys.*, vol. 21, pp. 76–79, 1984.
[18] A. J. Surowiec, S. S. Stuchly, J. R. Barr, and A. Swarup, "Dielectric properties of breast carcinoma and the surrounding tissues," *IEEE Trans. Biomed. Eng.*, vol. BE-35, pp. 257–263, 1988.
[19] A. M. Campbell and D. V. Land, "Dielectric properties of female human breast tissue measured in vitro at 3.2 GHz," *Phys. Med. Biol.*, vol. 37, pp. 193–210, 1992.
[20] W. T. Joines, Y. Z. Dhenxing, and R. L. Jirtle, "The measured electrical properties of normal and malignant human tissues from 50 to 900 MHz," *Med. Phys.*, vol. 21, no. 4, pp. 547–550, 1994.
[21] M. Lazebnik, L. McCartney, D. Popovic, C. B. Watkins, M. J. Lindstrom, J. Harter, S. Sewall, A. Magliocco, J. H. Booske, M. Okoniewski, and S. C. Hagness, "A large-scale study of the ultrawideband microwave dielectric properties of normal breast tissue obtained from reduction surgeries," *Phys. Med. Biol.*, vol. 52, pp. 2637–2656, 2007.
[22] M. Lazebnik, L. McCartney, D. Popovic, C. B. Watkins, M. J. Lindstrom, J. Harter, S. Sewall, T. Ogilvie, A. Magliocco, T. M. Breslin, W. Temple, D. Mewand, J. H. Booske, M. Okoniewski, and S. C. Hagness, "A large-scale study of the ultrawideband microwave dielectric properties of normal, benign, and malignant breast tissues obtained from cancer surgeries," *Phys. Med. Biol.*, vol. 52, pp. 6093–6115, 2007.
[23] A. Stogryn, "Equations for calculating the dielectric constant of saline water," *IEEE Trans. Microwave Theory Tech.*, vol. MTT–19, pp. 733–736, 1971.